EFFECTIVE TEMPERATURE BASED ALGORITHM FOR ACHIEVING CONSTANT QUALITY RESISTANCE SEAM WELD

by

Miroslav M. MIJAJLOVIĆ[a,*], Dušan Z. ĆIRIĆ[a], and Sonja M. VIDOJKOVIĆ[b,c]

[a] Faculty of Mechanical Engineering, University of Nis, Nis, Serbia
[b] Faculty of CEG – Watermanagement Department, TU Delft, Delft, Netherlands
[c] Institute of CTM, University of Belgrade, Belgrade, Serbia

Original scientific paper
https://doi.org/10.2298/TSCI200307222M

The resistance seam welding is a welding technique that is often used for the creation of the leak-tight welds. It is a technique where the weld is created as a set of overlapping weld nuggets between the cylindrical welding electrodes. The creation of the weld nuggets is depending on many external and internal parameters. Some of the external parameters are pressing force, welding electrodes, electrical current and time, while the internal parameters are electrical resistance, resistivity, and temperature. The main issue with the resistance seam welding is to properly set up internal and external parameters, create a weld nugget of a certain quality, reconfigure the parameters, relocate, and create another weld nugget of the same quality. The modern welding machines must have monitoring systems capable to make decisions and recalibration of the parameters. These systems are very complex and expensive, and as such, non-affordable for many small enterprises. This paper is presenting an effective, temperature-based algorithm for selecting the optimal welding parameters before the welding begins. The algorithm bases on the data from the experimental welding and numeric simulation of the welding process. The verification of the algorithm is done after testing the quality of the welds.

Key words: *resistance seam welding, temperature, algorithm, quality*

Introduction

The resistance welding, defined as ISO 4063 – 2 welding process [1], represents a group of the welding processes that use the electric current, electric resistivity of materials, and electric resistivity of contacts to generate the heat necessary for welding. It is a local joining process, usually used for the sheet-shaped workpieces – only a small volume of the material will melt and solidify again into the weld nugget. The electrical current is discrete, in short bursts, delivered to the workpieces over the copper electrodes which press the workpieces one to another. When properly set, the workpieces initially heat between the electrodes, locally melt, and weld one to another. When finished, the electrodes move to another location and repeat the procedure.

A special group of the resistance welding processes is a lap seam resistance welding, defined as ISO 4063 – 221 welding process [1]. The main characteristics of the 221 process is the use of the cylindrical copper wheels as electrodes which press the sheets, roll over them,

* Corresponding author, e-mail: miroslav.mijajlovic@masfak.ni.ac.rs

and do not stop pressing the sheets when changing the welding location. When welding parameters are properly set, the creation of the discrete weld nuggets happens close one to another (or partially overlapping one to another) what results in continual and leak-tight seam welds (when nuggets overlap).

The main issue with the 221 welding process is a necessity to guide, monitor, and control the welding sequence from weld nugget to weld nugget. The modern concepts of the monitoring in 221 consider monitoring the electric current, pressing force, sheet displacements, and sequence duration. They can be monitored separately, or in pairs, or all of them. However, their monitoring requires a very complex and very expensive computer and measuring systems. The data processing, decisions making, and proactive behavior make the situation even more complex [2].

A recent trend in 221 welding is simplification of the systems, where such behavior is suitable. Several authors clearly indicate that the electrical current is of a major influence on the quality of the weld nugget. Mira-Aguiar *et al.* [3] have recently reported the expulsion of the zinc in the galvanized steel sheets welded using 221. In their opinion, the better control of the welding electrical current is a must for qualitative welding. Ma *et al.* [4] give a review of monitoring techniques in two welding processes. As a main parameter, they recognize the power input into the process and the temperature as a main qualitative parameter that defines the size of the weld nugget. They find that destructive tests of the welds as the only valid method to determine if the welding process was properly performed. Zhao *et al.* [5] use both experimental and numerical researches to get optimal welding parameters while spot welding dual-phase steel. They recognize enthalpy of the welding process as the main parameter to optimize to reach optimal weld nugget size. Jaber *et al.* [6] have found that the greater electrical current used than optimal might displace the location of the pressing force in 221 welding. There is presented a dependency of the electrical current and the displacement effect but it is limited for a specified work case given in the paper.

Kaščak and Spišak [7] evaluated the influence of the welding current on the surface quality of the high-strength steels. Their research was aiming the resistance spot welding, but the conclusions are universal for all resistance processes: the lower value of the electrical current does not lead to the expulsion and overheating of the workpieces. When welding current is too high, the quality of the weld nuggets decreases, the expulsion appears and it is necessary to intensively cool-down the workpieces. Therefore, in the case of the resistance seam welding, the monitoring and in-time welding parameters optimization is a prerogative for the qualitative welds.

Almost all of the authors that have been dealing with the resistance seam welding point out the problem of real-time monitoring and adaptation of the welding parameters. The main issues they are dealing with are complexity, response time, and prices of the system. Here is presented a simple, temperature-dependent algorithm for prescribing and selecting the optimal welding parameters that might be useful for a certain seam welding cases.

Algorithm for selecting optimal welding parameters

In general, the leak-tight seam weld consists of a number of overlapping welded spots (nuggets) that are created during resistance spot welding. The weld nugget is a small (usually ellipsoidal) volume of the base material that has been molten and afterward solidifies between the workpieces. As such, it is a localized, solid bond between workpieces. The crea-

tion of the following nugget requires the local melting of the workpieces and partial melting of the previous nugget, as well.

Basically, the weld nugget is the volume of workpieces between the welding electrodes (wheels) defined with the temperature. The temperature of the weld nugget, in the moment of creation, varies between the minimal, $T_{\min}$, and maximal temperature, $T_{\max}$. The isosurface of the minimal temperature defines the size, shape, and boundary of the welding nugget. The maximal temperature usually appears at the nugget's center of gravity. It has to be higher than the melting temperature of the harder material. When two dissimilar materials are to be welded, the material of the weld nugget is a mixture of both materials with a melting temperature between softer and harder materials' melting temperatures. Therefore, the minimal *welding* temperature has to be higher than the melting temperature of the nugget's mixture.

Theoretical electrical current used in the resistance seam welding should be continuous (direct current), having *on* and *off* regimes (with and without electrical current) within one welding cycle. It is necessary to point out that optimal welding nugget does not have to be created within one welding cycle. However, the use of direct current shows several disadvantages: low-quality welds, extreme heating, unnecessary use of energy and it requires a very robust welding machine. More often, alternating currents with quasi-sinusoidal shapes are used, having *on* and *off* regimes, as well. It is important that effective electrical current for alternating current $\tilde{I}_{\text{ef}}$, in sum, has the same value as theoretical, direct current's effective value $\bar{I}_{\text{ef}}$. When symmetrical alternating current used, the maximal value of the alternating current $\tilde{I}_{\max}$ has significantly greater value than the maximal value of the direct current $\bar{I}_{\max}$.

Considering the energy input (as electrical current given *vs*. time in the figs. 1(a) and 1(b), the optimal temperature at the boundary of the nugget should be as given in fig. 2(a) for direct current and in fig. 2(b) for the alternating current.

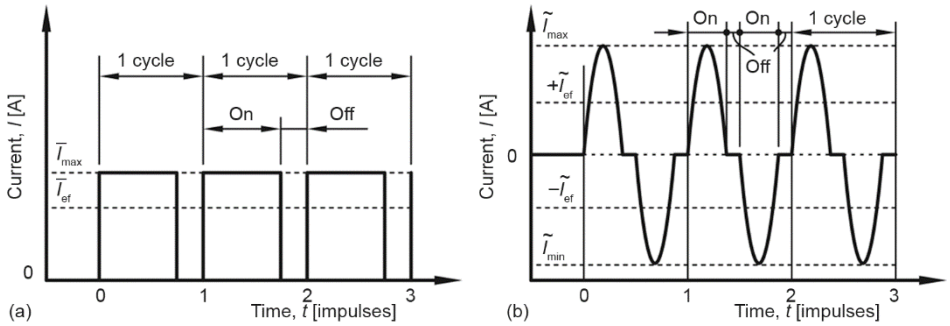

Figure 1. Electrical current; (a) theoretical sequence and (b) realistic sequence

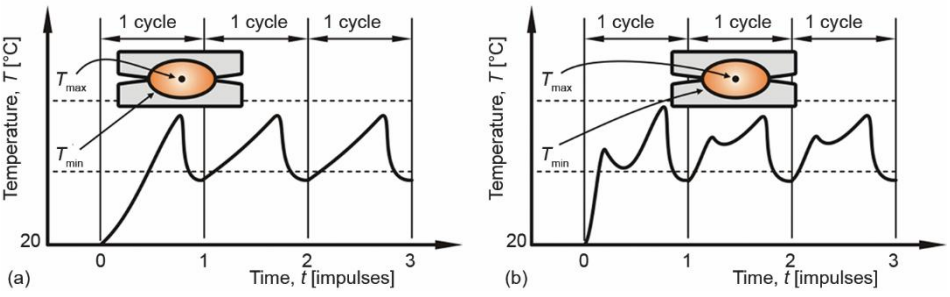

Figure 2. Maximal temperature in the weld nugget; (a) for theoretical sequence and (b) for realistic sequence

Assuming that the weld nugget is created during the one-time cycle, it is clear that there has to be a difference in the energy input for the first and the following welding nuggets to keep the temperature of the weld nugget within the optimal temperature range. Furthermore, knowing that many factors influence the heat generation at the contact interfaces, the management of the welding nugget's temperature is a challenging task.

The heat generation at the contacts is directly defined by the welding electrodes, electrical current, pressing force of the electrodes and the time. All of them influence the resistivity and the resistance of the contacts and what is affecting the heat input into the weld. Some of them, as electrical current, directly affect the heat input. Time is the only parameter that directly and indirectly influences all of the heat-generating parameters. If the forced cooling mechanisms (*e.g.* cooling water) are not used, the time, combined with the electrical current in the off-stage, is the only parameter that manages the cooling. This is essential for the optimal nugget and leakage-tight weld creation.

Therefore, to create an optimal weld nugget, the parameters that influence the nugget's temperature have to be adjusted before the creation of the new nugget starts.

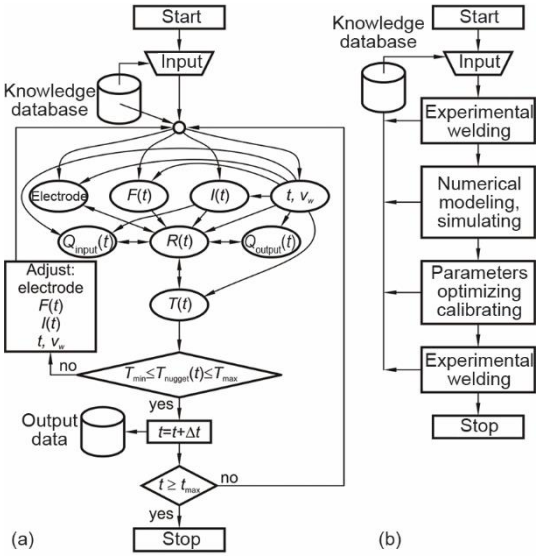

Figure 3. Algorithm; (a) temperature field estimation and (b) conceptual algorithm

Figure 3, a shows the simplified schematic of the mutual dependencies between parameters that affect the nugget's temperature and a principal algorithm of the optimal nugget's creating. In the initial step of the algorithm use, the knowledge database is filled with the relevant data – temperature extremes (and characteristic values) for the materials in contact, data about the electrodes, welding machine, and operational data – welding current, welding time, welding cycle, initial contacts, resistivity, empirical data about the similar welding cases, *etc.* Setting up the proper knowledge database is usually a long lasting and demanding task. The intelligent units of the algorithm immediately create mutual dependences between the insert data. Afterwards, the working parameters are used as the initial data – the temperature field, *T*-field, is calculated and compared to the prescribed optimal *T*-field of the ideal working configuration. If needed, what is in major situations a must, the input data are calibrated (changed, increased, decreased, and adjusted) to inflict more suitable *T*-field for the realistic working configuration/conditions. When weld nugget's *T*-field stabilizes within the prescribed temperature range, creation of the new weld nugget starts. The initial data (contacts, *T*-field, loading, *etc.*) for this case are the last calculated data (from the last optimal welding cycle).

An effective algorithm of welding (and selection of the welding parameters) is incorporated in a real-time computing system combined with the welding machine. The machine provides the real-time welding process parameters (*e.g.* temperature, force, welding current, time – the number of *on* and *off* cycles, welding duration, welding speed, *etc.*) and transfers it to the calculation and calibrating system. Welding of a single nugget is performed using

the given parameters. The welding machine makes a quick weldability status test – temperature measuring, force, and welding current stability. Afterwards, it recalculates what would happen (for example, with the *T*-field) if some of the parameters have been fine-tuned (*e.g.* welding current's maximal value). When the temperatures are not within the prescribed range, the system promptly selects new *optimal* welding parameters, calculates the effect of the application of these parameters. If the results are giving satisfactory results, the system calibrates the welding machine to work with these new parameters. Afterward, the welding machine would perform the welding and procedure of recalculation and calibration should be proceeded again. The algorithm for optimal parameter selecting partially uses fuzzy logic, sequential neural network and repetitive learning methods.

Such a system is extremely complex (and expensive to build) and state of the art calculation systems are incapable to perform almost instant calculations of the temperature fields in the weld nuggets and workpieces.

The more realistic concept is a combination of the preliminary experimental welding, optimization/calibration of the process within the numerical model/simulation and validation on the following experimental welding. The conceptual algorithm of such a system is given in fig 3(b). The estimation/definition of the workpiece's temperature field is an essential part of this algorithm.

Temperature field

The temperature field of workpieces can be obtained as a solution of the heat equation:

$$\rho_v c_p \frac{\partial T}{\partial t} - \nabla(k\nabla T) = \dot{q}_v \tag{1}$$

where ρ_v [kgm^{-3}] is the density, c_p [Jkg^{-1}K^{-1}] – the specific heat, T [K] – the temperature, t [s] – the time, k [Wm^{-1}K^{-1}] – the thermal conductivity, and $\dot{q}_v$ [Wm^{-3}] – the volumetric heat source.

The volumetric heat sources are the contact pairs upper electrode-workpiece 1, workpiece 1-workpiece 2, workpiece 2-lower electrode and workpieces itself, but significantly less than contact pairs. In sum, they deliver heat $\dot{Q}_v$ [W] into the control-volume. By the Ohm's and Joule's laws, the generated heat $\dot{Q}_v$ is:

$$\dot{Q}_v = RI^2 \tag{2}$$

where R [Ω] is the electrical contact resistance and I [A] – the electrical current.

The total energy delivered to the control volume Q_v [J], delivered during time interval of t is:

$$Q_v = RI^2 t \tag{3}$$

The electrical contact resistance and the electrical current are time-dependent values:

$$Q_v = \int_0^t R(t)I^2(t)\mathrm{d}t \tag{4}$$

where $R(t)$ [Ω] is the electrical contact resistance dependent on t and $I(t)$ [A] – the electrical current dependent on t.

The time dependent electrical contact resistance at the contact side of the body, i, R_i [Ω] is:

$$R_i(t) = \frac{\rho_i(t) l_i(t)}{A(t)} \tag{5}$$

where $\rho_i(t)$ [Ωm] is the electrical contact resistivity at i side of the body, $l_i(t)$ [m] – the film thickness of the contact area at i side, and A [m^{-2}] – the load-bearing contact area. It is assumed that, due to the surface roughness, the load-bearing contact area is only 25-30% of the nominal contact area A_n.

Therefore, when two bodies have contact over the contact pair 1 and 2, the total electrical contact resistivity, $\rho(t)$, is [8]:

$$\rho(t) = 3\xi \left\{ \left[\frac{\sigma_{\text{soft}}(t)}{\sigma_{\text{n}}(t)} \right] \left[\frac{\rho_1(t) + \rho_2(t)}{2} \right] + \rho_{\text{c}}(t) \right\} \tag{6}$$

where ξ [–] is the constant, from 0.1 to 10, $\sigma_{\text{soft}}(t)$ [Nm^{-2}] – the time and temperature dependent flow stress of the softer material from the contact of 1 and 2, $\sigma_{\text{n}}(t)$ [Nm^{-2}] – the contact pressure, $\rho_1(t)$, $\rho_2(t)$ [Ωm] – the resistivity of the contact pair 1 and 2, respectively at sides 1 and 2, and $\rho_{\text{c}}(t)$ [Ωm] – the resistivity of the contaminant between 1 and 2, if any contaminant present.

Empirical data

The welding time (the time period necessary to create one solid nugget) is a very important parameter in resistance seam welding. If weld time is less than optimal, there is insufficient time for proper heat flow inside the weld. As such, the weld will begin to exhibit adiabatic nature (premature heat loss), nugget size instability, and material expulsion [9]. By the same measure, if weld time is too long, the weld nugget does not benefit. However, the welding electrodes unnecessary heat up, waste energy and rapidly wear down. Empirically obtained optimal by [9], for one-nugget, welding time t_{n} [second] of the structural low-carbon steel sheets is:

$$t_{\text{n}} = 0.0292 s^2 \tag{7}$$

where s [mm] is the total width of the sheets to weld, fig. 4

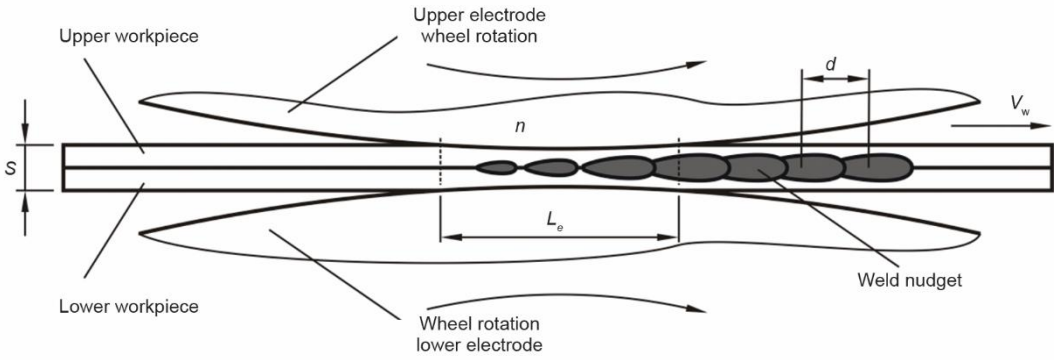

Figure 4. Resistance seam welding electrodes in contact [9], retouched image

The proper definition of the resistance seam welding cycle also depends on the electrode footprint length, L_e, fig. 4. When alternating current is applied for the welding (what is the most common situation), the welding time can be estimated as:

$$t_n = \frac{n}{f} \tag{8}$$

where n is the number of weld nuggets below the welding electrode, within the footprint length at any time. The number of nuggets is mostly n = 1-4.

To create leak-tight seam welds, empirical researches on low-carbon steel sheets show that optimal distance between nuggets d [mm] should be in the range [9, 10]:

$$1.5s \leq d \leq 2.5s \tag{9}$$

Afterward, the electrode footprint L_e [mm] can be estimated as:

$$L_e = dn \tag{10}$$

Finally, the welding speed v_w [mms^{-1}] is:

$$v_w = dt_n \tag{11}$$

The rest of the data, important for the welding of typical low-carbon steel is given in tab. 1.

Table 1. Recommended welding parameters for the steel 1.0570 [11]

Sheet thickness [mm]	Pressing force [kN]	Electrode face width [mm]	Welding current [kA]	Weld time cycles [–]	Press-off time cycles [–]	Weld distribution [nuggets per cm]	Welding speed [mmin^{-1}]
0.8-1.0	4.0	5	12	2	2	4	1.8
1.0-1.2	4.8	5.5	14	3	2	3.5	1.7

Finally, the empirical data and recommendations should be always tested for the applicability of a certain, specific problem.

Numerical simulation, experimental results, and discussion

The object of interest of the research was the plate and shell heat exchanger and welding of the central segment. The segment is made of two symmetrical, 1 mm thick steel sheets, a diameter of 180 mm, having 30 heat-exchange ribs [12]. The contact surface of the sheets is at the periphery flat surfaces. Before this welding attempt, the sheets were commercially welded using the TIG welding process (ISO 4063 – 141) at the outer edge of the sheet. The resistance seam welding (ISO 4063 – 221) is planned to be done in the middle of the contact surfaces.

For the numerical modeling, the computer-aided design model of the heat exchanger (2 complex parts) is sliced into many simpler pieces (420 simpler parts) to enable the creation of 320426 high-qualitative HEX elements with no wedge or tetrahedral elements created, fig. 5(a). The sheet is discretized with two elements per sheet thickness but local refinement in the zone of welding is activated what doubles the number of elements with a factor of two (four elements per thickness). The ratio of HEX elements (max element length divided min element length) is set to be maximally 3.

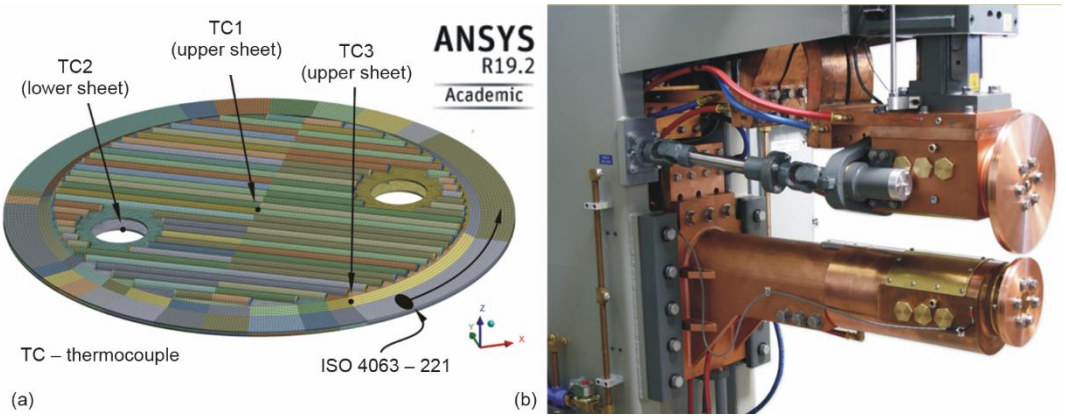

Figure 5. Resistance seam welding; (a) discretized computer aided model and (b) welding machine RSW AA-3KM P used for the experiments

The initial (non-adapted) welding has been numerically simulated using a straight-lined alternating current shape (triangle shaped) with an effective value of $\tilde{I}_{ef}$ = 5100 A, which is a recommended value and gives the leak-tight seam weld. Considering the empirical recommendations, the optimal welding time per weld nugget in such a configuration should be t_n = 0.1168 seconds. It is acceptable to have a welding sequence of 5 cycles plus 1 cycle for entering and leaving the welding sequence (t_n = 0.12 seconds for a frequency of 50 Hz) where the first cycle starts at time 0.005 seconds. The first full three cycles are the *current on* cycles, where the first 75% of each half-cycle is having a changeable electrical current, while the last 25% of the cycle is with a constant electrical current of zero. The maximal welding current is $\tilde{I}_{max}$ = 13600 A. The last two full cycles plus the rest time of the one entering/leaving cycle are *current off* used for cooling the weld nugget. The pressing force of the electrode wheels is accepted to be a constant value of F_p = 3500 N, active during the complete welding sequence. The electrical current and the pressing force are given in fig. 6.

The distance between the weld nuggets is d = 2.7s, which gives the constant n = 3.1 weld nuggets between the electrode wheels at every moment and the electrode footprint of L_e = 8.37 mm. The shape and dimensions of the electrode wheels are given in fig. 7.

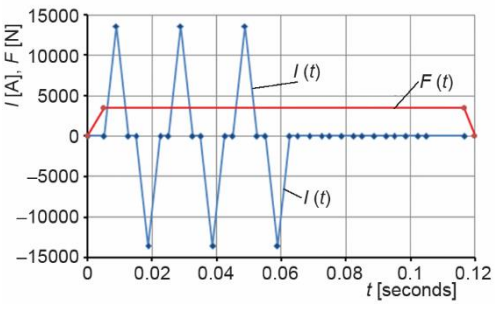

Figure 6. Used welding parameters – pressing force and electrical current

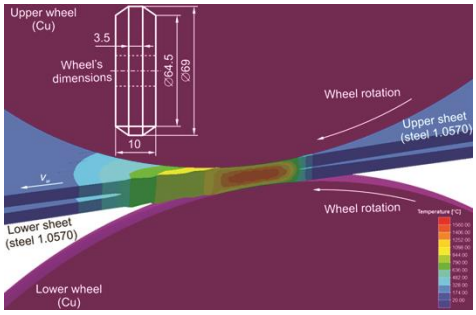

Figure 7. Temperature field of the workpieces and dimensions of the electrode wheels

After the simulation, the initial experimental welding on the sheets, fig. 5(b), with the prescribed welding parameters, has been performed, as well.

Afterward, the numerical simulation of the welding, with the activated algorithm for the temperature adaptation, is performed. Due to the complexity and duration of the simulation, the adaptation criteria is set only on changing the effective welding electrical used current per weld nugget. This means that the welding duration, press force and the structure of the welding sequence (number of the welding cycle, current on and off duration/ratio) are preserved as constant, but there is an option to activate them for better tuning of the welding process.

For proper adaptation of the welding current per weld nugget, with a goal to reach the temperature of the weld nugget within the prescribed minimal and maximal temperature, it was necessary to perform 19 to 28 adaptations of effective electrical current and the algorithm has performed the same number of simulations per weld nugget.

Figure 7 shows the temperature field of the welded sheets (section view) during the welding of the sixth welding node (at t = 0.65 seconds). At this moment, the sheets are cold, except in the welding zone.

Figure 8 shows the used effective electrical current used per weld nugget for the first 100 nuggets (what is approximately 320 m of welded length, while complete welded length is 560 mm).

Figure 9 presents the maximal temperature of the welding nugget for the non-adapted effective electrical current (first numerical simulation, first case) and the adapted effective electrical current (second numerical simulation, second case).

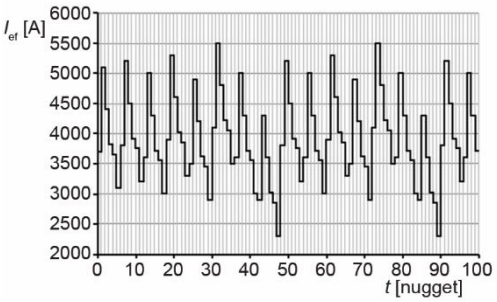

Figure 8. Effective electric current used for adapted experimental welding

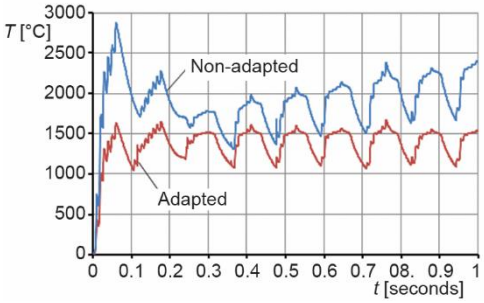

Figure 9. Simulated maximal temperatures of the welding nuggets for non-adapted and adapted cases

The temperature of the weld nuggets in the first case is significantly higher than the melting temperature of the steel 1.0570 (1508 °C). However, this is not as important as the fact that the maximal temperatures of weld nuggets dramatically different from one to another. Also, there is a trend of sheet overheating as the welding process goes and there is a need for intensive water cooling to preserve the integrity of the plates. On the other side, the use of adapted effective electric current in the second case gives the nuggets maximal temperature slightly higher than the sheet's melting temperature. The temperatures of the weld nuggets are much closer one to another, as well.

Figure 10 shows the macro-structure of the achieved seam welds in the first case, fig. 10(a) and the second case, fig. 10(b). The sample in the figure is taken for the unfinished weld, approximately at the half of the prescribed welding length (fast stop technique – the welding current is cut-off and the electrode wheels are instantly moved away from the welding zone). The first observation is that the expulsion of the molten material in the zone of the last weld nugget is significantly larger for the first case than for the second case. It is, also,

notable that the height of the weld nugget is larger for the first case, but the squeezing of the welded sheets is larger in the second case. Obviously, the larger expulsion of the molten metal (affected by the more intensive melting), relaxes the deformation of the welded sheets in the width-direction what is not happening in the second case welding.

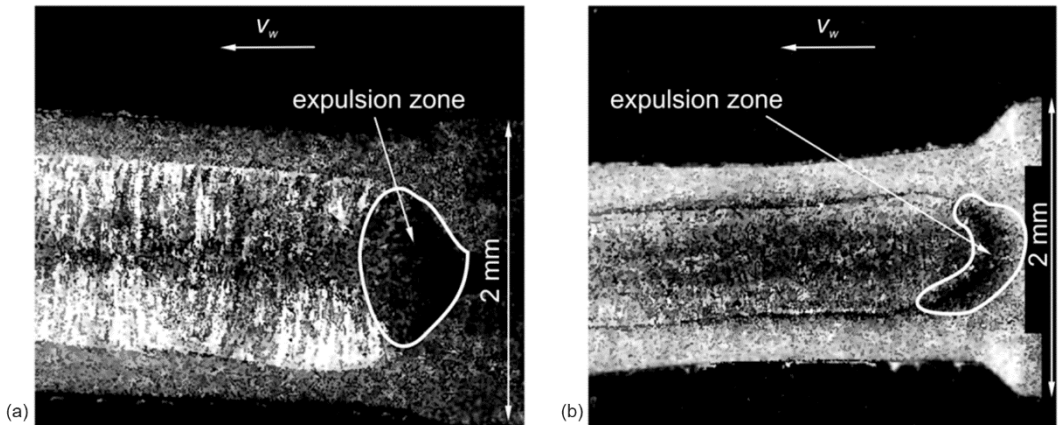

Figure 10. Macro-structure of the weld nugget for; (a) non-adapted welding and (b) adapted welding

Table 2 shows the average dimensions of the weld nuggets. All of the analyzed nuggets are ellipsoidal (almost identical ellipses in all three *xyz*-section cuts), differing in axis lengths. All of the examined nuggets slightly differ in size (less than 3%) for the non-adapted case of welding while adapted welding cycle shows minor size difference (less than 1%). The average dimensions in tab. 2 are estimated from the 12 analyzed nuggets, at different locations on the welded workpieces.

Table 2. Comparison of the major results for adapted and non-adapted welding cycles

Case	Weld nugget		Temperature difference		
	Shape [–]	Average dimensions *x*, *y*, *z* [mm]	At TC1 [°C]	At TC2 [°C]	At TC3 [°C]
Non-adapted	Ellipsoid	2.15/4/2.1	Max. 4	Max. 6	Max. 15
Adapted	Ellipsoid	2.05/2.55/2.1	Max. 4	Max. 2	Max. 11

Finally, the validation of the proposed algorithm/simulation for adaptation/optimization of the welding parameters is done comparing the temperatures from the numerical simulation and experimental welding in three independent points at workpieces. The temperature during welding is measured using the TC located as shown in fig. 5(a). Figure 11 shows the temperatures measured at TC1, TC2, and TC3 compared to the temperatures of the nodes from the adapted numerical simulation (for first 6 seconds of welding). The temperatures at TC1 and TC2 differs from the numerically obtained temperatures for less than 2 °C (not shown in fig. 11 to simplify the view),

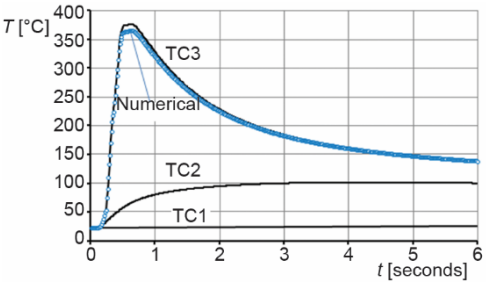

Figure 11. Temperatures at TC *vs.* numerical temperatures at prescribed nodes

while the temperature difference at TC3 differs from the numerical temperature of adequate note maximally 11 °C (tab. 2).

Conclusion

The leak-tight resistance seam welds can be created without the use of the expensive monitoring and decisions making systems, but the constant quality of the weld can be achieved only if the welding parameters are varied and optimized. The temperature of the workpieces in the zone of the weld nugget defines the shape, size, and quality of the weld nugget. Therefore, keeping the temperature of the weld nugget within prescribed boundaries is of greatest importance. It is found suitable to make experimental welding(s), use the results within the numerical simulation, and define the optimal welding parameters for each welding nugget before the welding starts.

Acknowledgment

This research was financially supported by the Ministry of Education, Science and Technological Development of the Republic of Serbia.

References

[1] *** SRPS EN ISO 4063: Welding and Allied Processes, Published 28.01.2013
[2] Westgate, S. A., Resistance Welding-State of the Art, *Wel. and Cut., 55* (2003), Mar., pp. 256-260
[3] Mira-Aguiar, T., *et al*., Solid-State Resistance Seam Welding of Galvanized Steel, *Int. J .Adv. Manu. Tech., 86* (2016), 5, pp. 1385-1391
[4] Ma, Y. *et al.*, Review on Techniques for On-Line Monitoring of Resistance Spot Welding Process, *Adv. in Mat. Sci. and Eng., 2013* (2013), ID 630984
[5] Zhao, D. *et al.*, Modeling and Experimental Research on Resistance Spot Welded Joints for Dual-Phase Steel, *Materials, 12* (2019), 7, ID 1108
[6] Jaber, H. L. *et al.*, Peak Load and Energy Absorption of DP600 Advanced Steel Resistance Spot Welds, *Iron & Steel, 44* (2017), 9, pp. 699-706
[7] Kaščak, L., Spišak, E., Evaluation of the Influence of the Welding Current on the Surface Quality of Spot Welds, *The International Journal of Engineering and Science, 5* (2016), 12, pp. 32-37
[8] Bay, N., Wanheim, T., Real Area of Contact Between a Rough Tool and a Smooth Workpiece at High Normal Pressure, *Wear, 38* (1976), 2, pp. 225-234
[9] ***, ASM Handbook Volume 6: Welding, Brazing, and Soldering (eds.: D. L. Olson, T. A. Siewert, S. Liu, G. R. Edwards), ASM, New York, USA, 1993
[10] Kulkarni, A. S., Inamdar, K. H., Effect of Process Parameters on Resistance Welding, *Int. J. Eme. Tech. Inn. Res., 2* (2015), 4, pp. 963-967
[11] ***, Ruukki, https://www.scribd.com/document/93507084/Ruukki-Resistance-Welding-Manual
[12] ***, Euroheat, https://www.euroheat.co.rs/catalog/izmenjivaci-toplote/plocasto-dobosasti/

Paper submitted: March 7, 2020
Paper revised: July 22, 2020
Paper accepted: July 26, 2020